

LETTER TO THE EDITOR

Gaia DR2 orbital properties for field stars with globular cluster-like CN band strengths

A. Savino¹ and L. Posti^{1,2}

¹ Kapteyn Astronomical Institute, University of Groningen, Postbus 800, 9700 AV Groningen, The Netherlands. e-mail: A.savino@rug.nl

² Observatoire Astronomique, Université de Strasbourg, CNRS, 11, rue de l'Université, F-67000 Strasbourg, France. e-mail: lorenzo.posti@astro.unistra.fr

Preprint online version: March 7, 2022

ABSTRACT

Context. Large spectroscopic surveys of the Milky Way have revealed that a small population of stars in the halo have light element abundances comparable to those found in globular clusters. The favoured explanation for the peculiar abundances of these stars is that they originated inside a globular cluster and were subsequently lost.

Aims. Using orbit calculations we assess the likelihood that an existing sample of 57 field stars with globular cluster-like CN band strength originated in any of the currently known Milky Way globular clusters.

Methods. Using Sloan Digital Sky Survey and Gaia data, we determine orbits and integrals of motion of our sample of field stars, and use these values and metallicity to identify likely matches to globular clusters. The pivot hypothesis is that had these stars been stripped from such objects, they would have remained on very similar orbits.

Results. We find that $\sim 70\%$ of the sample of field stars have orbital properties consistent with the halo of the Milky Way; however, only 20 stars have likely orbital associations with an existing globular cluster. The remaining $\sim 30\%$ of the sample have orbits that place them in the outer Galactic disc. No cluster of similar metallicity is known on analogous disc orbits.

Conclusions. The orbital properties of the halo stars seem to be compatible with the globular cluster escapee scenario. The stars in the outer disc are particularly surprising and deserve further investigation to establish their nature.

1. Introduction

One of the major challenges in modern stellar population studies is to understand the origin of multiple stellar populations that are found in globular clusters (GCs). This phenomenon consists of specific elemental abundance variations within a given cluster that are not easily accountable for in the framework of stellar nucleosynthesis and chemical enrichment (e.g. Bastian & Lardo 2018, and references therein). The typical chemical pattern consists of enhancement in He, N, and Na (sometimes Mg and Si), and depletion in C and O (sometimes Al). This distinctive pattern is so ubiquitous in massive GCs, and exclusive to them, that it is now considered a signature feature to include in the very definition of these stellar systems.

However, in the last decade evidence has accumulated that a fraction of stars in the Milky Way (MW) stellar field present very similar elemental abundances to those observed in GCs (e.g. Martell et al. 2011; Fernández-Trincado et al. 2017; Schiavon et al. 2017). As these chemical anomalies have been detected using a variety of low- and high-resolution spectral indicators, in the rest of this manuscript we will generally refer to these stars as ‘enriched’. As GCs are expected to lose mass through processes like evaporation and tidal stripping (e.g. Baumgardt & Makino 2003), the favoured hypothesis for the origin of enriched stars is that they were once part of a GC. However, this association has not yet been confirmed unambiguously.

Understanding the formation mechanism of these chemically peculiar stars in the MW has two potential rewards. It is currently accepted that the chemical anomalies of multiple stellar

populations arise only in the specific environment of a proto-GC where extremely high densities can be reached. This specificity is a stringent requirement of any formation scenario (e.g. Renzini et al. 2015). Establishing whether enriched stars in the MW field formed in a GC could either support the specificity requirement or reveal that multiple stellar populations can also form, to some extent, in lower density environments. On the other hand, identifying their birthplace can provide important details on the assembly history of the MW, in particular on the role of GC dissolution in that history.

To this end, the dynamical characterisation of known enriched stars can provide insight into their association with the GC system. Even though the spatial association among the components of a dissolving stellar system is quickly lost, kinematic coherence is much more long-lived and orbital parameters are not expected to change significantly for several Gyr (e.g. Helmi & White 1999). The first dynamical characterisation for a sample of enriched stars was performed by Carollo et al. (2013) and Fernández-Trincado et al. (2017). However, these studies employed ground-based proper motion measurements, resulting in relatively large uncertainties in the dynamical modelling. Thanks to the unprecedented precision reached by Gaia Data Release 2 (DR2) astrometric measurements (Gaia Collaboration et al. 2018a), we now have the chance to reconstruct the motion of enriched stars in much greater detail. This approach was taken by Tang et al. (2019) on a sample of CN-strong stars in the LAMOST survey. CN-strong stars are enriched stars that are identified through their strong absorption in the CN molecular band, thus suggesting enhancement in nitrogen.

In this paper we focus more closely on the suggested GC origin for these chemically atypical stars. We reconstruct the orbital properties for a sample of candidate enriched halo stars and compare them with a nearly complete sample of Galactic GCs, investigating the possible association. In § 2 we discuss our samples, in § 3 we describe our dynamical modelling, in § 4 we present our results, and we discuss the implications in § 5.

2. Data and sample selection

2.1. Enriched stars

For our analysis, we start from the sample of CN-strong stars from [Martell & Grebel \(2010\)](#) and [Martell et al. \(2011, hereafter M11\)](#). This is a sample of 65 CN-strong stars observed in the SEGUE and SEGUE-2 surveys ([Yanny et al. 2009](#)), selected to be metal-poor red giants. For these stars we recover the position in the sky, radial velocity, and metallicity from the Sloan Digital Sky Survey database, and other spectral and photometric parameters (see section 2.1.1).

We cross-correlate this sample with the Gaia DR2 database to obtain parallax and proper motion information. After the cross-correlation, and accounting for stars in common between the SEGUE and SEGUE-2 sample, we end up with 57 CN-strong stars for which we have six-dimensional phase-space information.

2.1.1. Distance determination

To perform a reliable dynamical modelling, accurate distances are needed for our CN-strong sample. Gaia parallax (ϖ) information can be used to get reliable distances; however, for this particular sample, simple estimators such as $1/\varpi$ or even more complex probabilistic approaches such as that of [Bailer-Jones et al. \(2018\)](#), which rely on disc-like priors for the MW stellar density distribution, are biased or simply not adequate.

[Martell et al. \(2011\)](#) provides distances to these stars by matching the dereddened $(g - r)_0$ colour to theoretical models for red giant stars of the appropriate metallicity. However, theoretical predictions for the colour of these stars are affected by uncertainties in many of the stellar model ingredients. This, combined with the steepness of the red giant branch tracks in the Hertzsprung-Russell diagram, can lead to potentially high systematics in the distance determination.

We thus rederived the distances to the 57 CN-strong stars using a more sophisticated approach. We built upon the Bayesian framework laid out by [Burnett & Binney \(2010\)](#) and evaluated the probability distribution that each star has a specific combination of distance, age, mass and metallicity based on the observed astrometric, spectroscopic and photometric properties.

As input observables, we use the dereddened g_0 magnitude and $(g - r)_0$ colour, and the spectroscopically derived T_{eff} , $\log(g)$, and $[\text{Fe}/\text{H}]$ values taken from the Sloan Digital Sky Survey database. We complement this information with the Gaia parallaxes. We use the alpha-enhanced BaSTI isochrones ([Pietrinferni et al. 2006](#)), covering the metallicity range $-3.62 \leq [\text{Fe}/\text{H}] \leq -0.29$, to estimate the multivariate Gaussian likelihood across our four-dimensional parameter space. The comparison between the expected and measured parallaxes takes into account the zero-point of -0.029 ([Lindgren et al. 2018](#)).

We estimate the final posterior probability distribution by combining the likelihood with priors on the physical parameters of the star. We use the recalibrated Kroupa mass function from [Aumer & Binney \(2009\)](#) as mass prior, combined with the

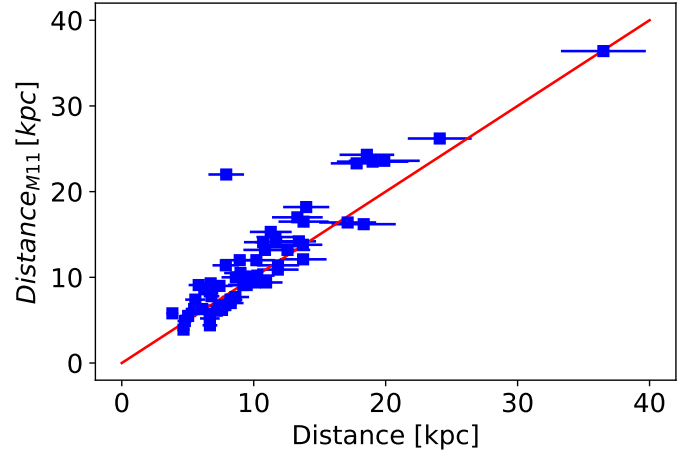


Fig. 1: Comparison between our Bayesian distance inference and the distances from [Martell et al. \(2011\)](#). The solid line marks the 1:1 relation.

three-component prior on age, distance, and $[\text{Fe}/\text{H}]$ from [Burnett & Binney \(2010\)](#). The best-fit stellar parameters and the related uncertainties are calculated from the first- and second-order moments of the probability distribution, respectively.

Figure 1 shows the comparison between our distance measurement and the M11 determination. Aside from one strong outlier (J224719.43+232144.9), the comparison is reasonable, with about 93% of our sample having heliocentric distance differences below 4 kpc.

2.2. Globular clusters

For the dynamical modelling of the GCs, we took the six-dimensional information from the catalogue of [Vasiliev \(2019b\)](#). This sample comprises 150 clusters; however, we excluded Djorg 1, Terzan 10, and ESO456-78 because of their highly uncertain radial velocities. We assigned an uncertainty to cluster distances of 2.3%, or 0.05 mag in distance modulus, as done in [Gaia Collaboration et al. \(2018b\)](#).

We adopted the cluster metallicities from [Carretta et al. \(2009\)](#); for the 15 clusters not present in this study, we took the metallicity from the catalogue of [Harris \(1996\)](#) (2010 version). Two clusters are not in the [Carretta et al. \(2009\)](#) sample or the [Harris \(1996\)](#) catalogue: Crater, for which we used the metallicity from [Kirby et al. \(2015\)](#), and 2MASS-GC03, for which we took metallicity and radial velocity from [Carballo-Bello et al. \(2016\)](#).

3. Orbital modelling

We integrate orbits and compute integrals of motion for both the stars and the clusters using AGAMA ([Vasiliev 2019a](#)). Some of the coordinate and velocity transformations make use of utilities from the Galpy ([Bovy 2015](#)) and Astropy ([Astropy Collaboration et al. 2013, 2018](#)) packages. We adopt the MW potential from [Piffl et al. \(2014\)](#), a multi-component axisymmetric model fitted to the kinematics of stars in the solar vicinity, which is also compatible with the most recent determinations of the dark matter halo virial mass from Gaia DR2 ([Watkins et al. 2018; Posti & Helmi 2019](#)). The adopted galactocentric coordinates for the Sun are $X_{\odot} = 8.3$ kpc, $Y_{\odot} = Z_{\odot} = 0$ kpc. The circular velocity at the solar radius is $V_{\odot}^{\text{Circ}} = 240.5$ km/s and for the

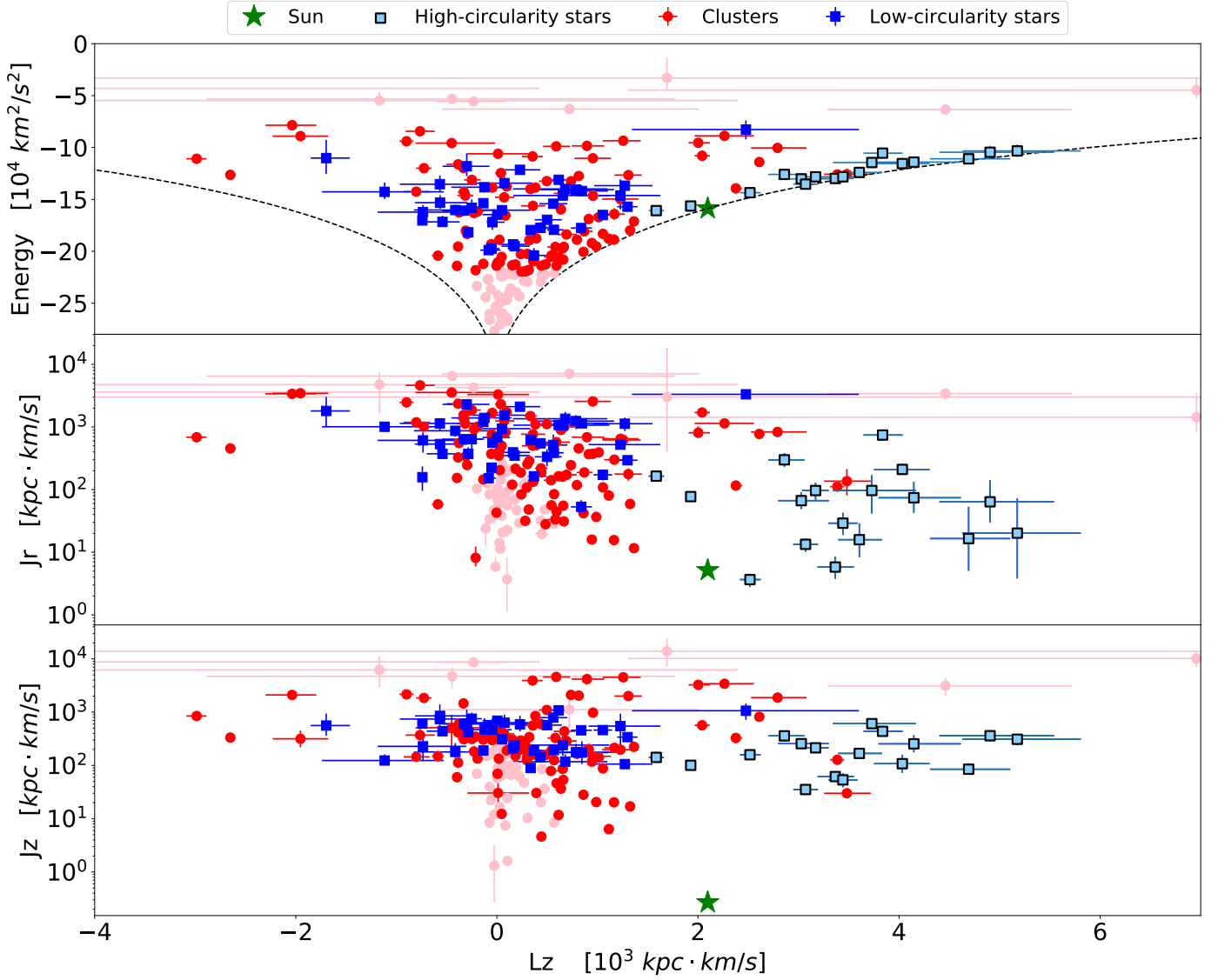


Fig. 2: Orbital energy (top), radial action (centre), and vertical action (bottom) as a function of the vertical angular momentum component for the globular clusters (red circles) and CN-strong stars (squares). Stars with circularity > 0.7 are shown in light blue and stars with circularity ≤ 0.7 are in dark blue. Clusters in pink are those with too high or too low orbital energy. The green star indicates the position of the Sun. The black dashed lines trace circular orbits.

peculiar velocity of the Sun we use $\mathbf{V}_{\odot}^{\text{Pec}} = [11.1, 12.24, 7.25]$ km/s (Schönrich et al. 2010).

For each star and GC we calculate the orbital energy E , the vertical component of the angular momentum L_z , and the radial and vertical actions J_r and J_z . The action integrals are computed via the ‘Stäckel Fudge’ approximation (Binney 2012). We integrate the orbit backwards in time, with a time-step of 10 Myr, up to a look-back time of 5 Gyr.

Uncertainties on the orbital parameters are computed with a Monte Carlo approach. For each star and cluster, we extract 1000 realisations for the position and the velocity, randomly sampling the uncertainties in the distance, radial velocity, and proper motion¹. The correlation between the two proper motions is taken into account, as is the systematic uncertainty of 0.035 mas/yr (Gaia Collaboration et al. 2018b). We thus construct the distributions of each quantity and associate its uncertainties by means of the 15.87 and 84.13 percentiles.

¹ The uncertainties on the sky position are assumed to be negligible.

4. Results

Figure 2 shows the integrals of motion for both the GC and CN-strong sample. The clusters span a much wider range of orbital energies than the CN-strong stars, thus we exclude clusters with $E < -2.2 \cdot 10^5 \text{ km}^2/\text{s}^2$ from the rest of our analysis. These clusters are confined in the inner regions of the Galaxy and are unlikely to be dynamically associated with our stellar sample. Similarly, also the distant clusters with $E > -7 \cdot 10^4 \text{ km}^2/\text{s}^2$ can be excluded². The excluded clusters are shown as the pink circles in Fig. 2.

While GCs smoothly occupy the region of low angular momentum orbits for a broad range of energies, the CN-strong stars seem to belong to two distinct orbital families. While most of the sample has integrals of motion compatible with halo kinematics (low $|L_z|$ and high E , J_r , J_z), another group of stars sits at

² Moreover, for these clusters the phase-space coordinates, and thus the integrals of motion, are very uncertain.

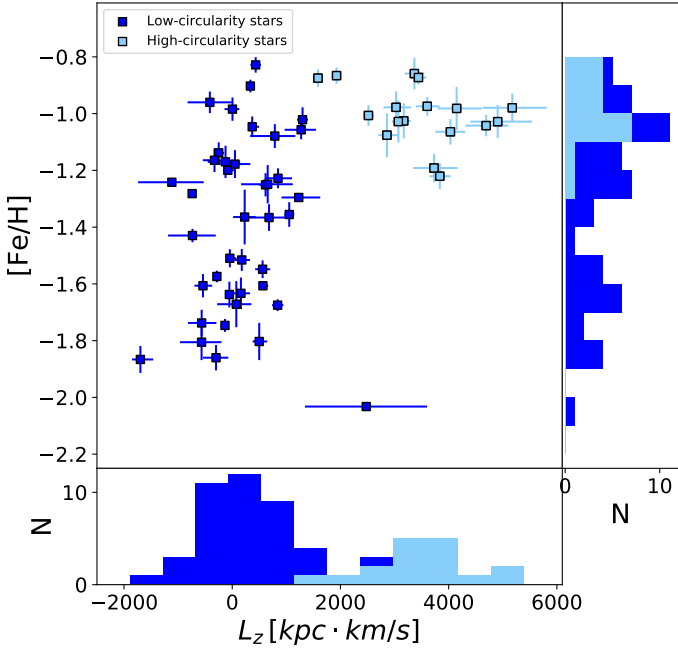


Fig. 3: Plot of L_z against metallicity for the CN-strong stars. Stars with circularity > 0.7 are shown in light blue, while stars with circularity ≤ 0.7 are shown in dark blue. The side panels show the distribution on the respective axis of the whole sample and of the high-circularity stars.

relatively high L_z for their energy. Their orbits are in fact very close to circular (dashed black line in Fig. 2; see also their trajectories in Fig. B.1), with typical galactocentric radii between 10 and 20 kpc and typical vertical excursions of a few kpc. We thus calculate the orbital circularity of the stars as

$$c \equiv \frac{L_z}{L_z^{\text{Circ}}(E)}, \quad (1)$$

where $L_z^{\text{Circ}}(E)$ is the angular momentum of the circular orbit at the same energy E of the star, and divide our sample into low-circularity stars ($c \leq 0.7$, dark blue squares in Fig. 2) and high-circularity stars ($c > 0.7$, light blue squares with black edges). The high-circularity stars have vertical actions and energies that are similar to the low-circularity stars, while having markedly higher angular momenta and smaller radial action, hence smaller eccentricities.

The 17 high-circularity stars, representing 29% of our sample of CN-strong stars, also differ from the low-circularity stars in their chemical composition. Figure 3 shows the L_z and $[\text{Fe}/\text{H}]$ distribution of our stellar sample. While the low-circularity stars are distributed roughly uniformly in metallicity, the high-circularity sample presents a very narrow metallicity distribution, peaking around -1.0. These stars in particular are found close to the upper limit of the metallicity selection adopted by M11, and thus we cannot exclude that we are seeing the low-metallicity tail of a larger, more metal-rich population. When comparing the kinematics of CN-strong stars with that of GCs, we find that the low-circularity stars lie in a region of the integrals of motion space that is compatible with some of the known MW GCs. Conversely, no cluster has orbital properties compatible with the high-circularity stars, with the exceptions of Pal1, E3, and ESO224-8. However, these clusters are significantly more metal rich ($[\text{Fe}/\text{H}] = -0.51, -0.73, \text{ and } 0.03$, respec-

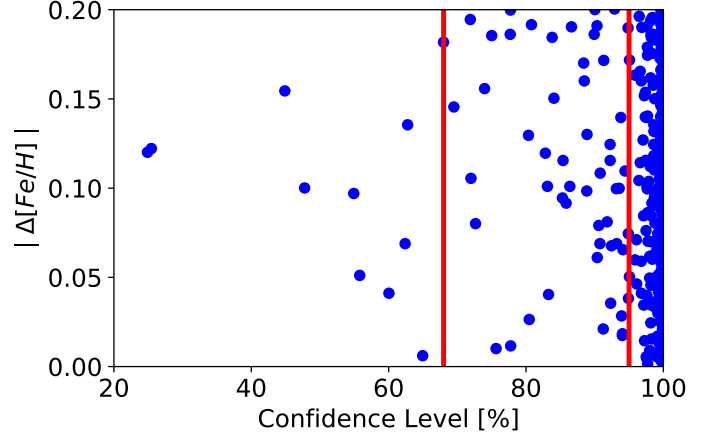


Fig. 4: For each cluster-star pair, confidence level for the pair to have different orbits against absolute difference in metallicity. Red lines indicate the 68% and 95% confidence level. Here the most likely star-cluster matches are those whose association can be rejected at a low confidence level.

tively) than our high-circularity sample, which means we can exclude them as the original birthplaces of these stars.

While Fig. 2 already shows that the low-circularity stars have orbits compatible with several GCs, the incredible precision with which the DR2 data allow us to recover the integrals of motion provides the opportunity to perform a much more detailed and quantitative comparison. Since actions are adiabatic invariants, stars that have escaped a GC would still have orbital actions that are very similar to that of the cluster itself. Thus, we compared the values of J_r , J_z , and L_z for every possible combination of CN-strong star and GC, totalling 5643 pairs. For each pair, we tested the null hypothesis that the cluster and the star have the same triplet of actions, taking into account the respective uncertainties. In Fig. 4 we show, for each star-cluster pair, the degree of confidence at which the hypothesis of dynamical association can be rejected versus the absolute difference in $[\text{Fe}/\text{H}]$. In order to be escapees from a given cluster, a CN-strong star must have the same value of $[\text{Fe}/\text{H}]$. However, to accommodate observational uncertainties, as well as possible zero-point offsets, we consider every pair with an absolute difference in $[\text{Fe}/\text{H}]$ less than 0.2 dex. The vast majority of orbital associations can be rejected at more than 95% confidence level. Only 63 cluster-star associations with compatible metallicity cannot be excluded at this confidence level and, among them, only 11 are below the 68% confidence level. These pairs are our best candidates for CN-strong star/GC association. We list the possible associations in table A.1. We note that while for 9 stars we find a likely association with just one cluster, for 11 others the null hypothesis is not rejected for several clusters. In these cases we cannot unambiguously identify an association, but we can still conclude that GCs were likely the birthplaces for these stars.

We finally note that we repeated our analysis using a different potential for the MW, as in McMillan (2017). We find very similar results to those presented here, with 60 pairs identified at the 95% confidence level.

5. Discussion and conclusions

In this letter we report on our dynamical characterisation of a sample of CN-strong red giants; we also compared their proper-

ties with those of the Galactic GC system to test the likelihood that these stars are cluster escapees.

We found that approximately one-third of our sample follows circular prograde orbits, with guiding radii of 10-20 kpc and vertical excursions of a few kpc. The orbital properties of the stars, and their relatively high metallicity, are much more similar to that of the Galactic thick disc, rather than to that of the stellar halo. The fact that some CN-strong stars from M11 are on disc-like orbits was already suggested by [Carollo et al. \(2013\)](#). However, the limited precision in their kinematic measurements prevented any stronger conclusion. The SEGUE footprint may play an important role in the selection of the outer thick disc envelope, and indeed Appendix B shows that many high-circularity stars are observed at their largest height from the Galactic plane (z_{\max}). It is curious to note that these stars are mostly located towards the Galactic anticentre, which is where the Galactic disc appears to be highly vertically perturbed ([Gómez et al. 2016](#); [Bergemann et al. 2018](#); [Laporte et al. 2018](#)).

The kinematics of the high-circularity stars is extremely different from that of any known GC (with the exceptions discussed in § 4). Given the available data, we cannot exclude that these stars have genuine GC-like abundances and trace a population of enriched stars unrelated to the current MW GC system. However, it is probable that these stars are contaminants in the selection of M11. At fixed metallicity and absolute magnitude (which are also known to affect the CN molecular feature used in M11), we note that the high-circularity stars are found to have the highest CN band strengths in our sample. This likely indicates that they have unusual compositions, and not that they are interlopers from the chemically normal field population.

For the origin of the high CN absorption, mass transfer from an asymptotic giant branch companion is a commonly invoked mechanism (e.g. [Schiavon et al. 2017](#)). Accretion from a massive ($3 - 8 M_{\odot}$) asymptotic giant branch star can enhance the atmospheric nitrogen abundance and mimic the light element pattern seen in GCs, but the fraction of field stars that undergo this enrichment process is expected to be low. Roughly two times the number of stars experience a similar process, with donors of $1.5 - 3 M_{\odot}$, and become CH-stars. These stars, characterised by high carbon abundance, also have strong CN absorption. As the selection from M11 is insensitive to carbon abundance at high metallicities, these stars are a likely source of contamination. Regardless of the donor mass, if binary mass transfer is the source of the chemical peculiarity in these stars, this could be confirmed by radial velocity monitoring. Unfortunately, the orbital periods of such binaries can be as long as many years ([Lucatello et al. 2005](#); [Starkenburg et al. 2014](#)), requiring long observational campaigns. Alternatively, high-resolution spectroscopy can provide the detailed abundance patterns of both light and s-process elements and validate the asymptotic giant branch pollution scenario.

In this letter we discuss how we tested, for each CN-strong star, the hypothesis that it is dynamically associated with any of the GCs. We did this by comparing the three orbital actions and the metallicity. We excluded the vast majority of cluster-star associations with a confidence level above 95%. However, 63 associations could not be excluded with such confidence. In particular, 7 stars had orbital and chemical properties that were very similar to those of at least one cluster, resulting in 11 promising star-cluster associations (see Table A.1, in bold). These stars may be among the first GC escapees robustly identified, not considering tidal structures observed around a few GCs. For this reason, we encourage high-resolution follow-up observations to confirm the chemical abundances.

The fact that 50% of our low-circularity CN-strong stars do not seem to be associated with any cluster in our sample does not necessarily refute the GC origin. There are a number of possible scenarios that can accommodate our findings. It is possible that some of our stars come from GCs that are not present in our analysis. While our GCs sample is nearly complete, it is certainly possible that we have not discovered some of the massive MW GCs, for example those lying beyond the highly extinct regions of the Galaxy. However, the number of still undiscovered clusters is expected to be very small ([Harris et al. 2013](#)).

A second scenario is that these stars come from long dissolved GCs. The idea of a population of GCs that have been completely dissolved by the MW tidal field gained support from the observation of strong mass loss in a few existing GCs ([Rockosi et al. 2002](#); [Odenkirchen et al. 2003](#); [Belokurov et al. 2006](#)) and it has found confirmation with the discovery of prominent, dynamically cold stellar streams in the halo of our galaxy ([Grillmair & Dionatos 2006](#); [Ibata et al. 2018](#); [Shipp et al. 2018](#)). Thanks to the wealth of information provided by Gaia DR2, several of these features have been detected ([Ibata et al. 2019](#)), suggesting that GC dissolution may be a rather common phenomenon. Furthermore, additional destruction channels have been proposed, such as dissolution in the turbulent discs of small galaxies, later accreted by the MW ([Kruijssen 2015](#)). Given the above arguments, GC destruction may play an important contribution to the population of CN-strong stars observed in the Galaxy. However, multiple populations arise only in GCs above a mass threshold of around $10^4 M_{\odot}$ ([Carretta et al. 2010](#); [Dalessandro et al. 2014](#); [Bragaglia et al. 2017](#); [Simpson et al. 2017](#)). Even above this threshold, the extent of light element variation and the fraction of enriched stars become larger with increasing mass ([Milone et al. 2017](#)). Hence, it is not clear whether cluster dissolution can be an efficient source of CN-strong stars in the MW field, given also that stars in more massive clusters are less easily stripped.

We also note an important caveat. In the case of the low-circularity stars, even if our dynamical analysis did not yield a conclusive association with any of the GCs, it is still possible that these stars were born in one of the GCs in our sample. This could be the case given the limitations of our dynamical approach, which assumes that there is equilibrium and that escapees retain orbital memory. The former might not be applicable, for instance in the case of a dynamically important accretion event, which can change the integrals of motions significantly; the latter does not happen if a star was expelled from the cluster at high velocity, for example after a three-body interaction.

In conclusion, even though we were able to assign one or more candidate parent clusters only to half of the low-circularity stars, the orbital properties of this subsample are broadly consistent with those of the halo GC population, supporting escape from GCs as a major formation channel for these stars. However, the inconsistency of such a scenario with the properties of high-circularity stars poses interesting questions. We strongly encourage follow-up analysis on these stars to unambiguously determine whether they are interlopers from a population of disc binary stars or if they have genuine GC-like abundances. In either case, the answer to this question will add precious information to the specificity hypothesis for GC multiple stellar population formation scenarios.

Acknowledgements. We wish to thank E. Balbinot, A. Helmi, D. Massari, and E. Tolstoy for the insightful discussions during the preparation of this manuscript. LP acknowledges financial support from a VICI grant from the Netherlands Organisation for Scientific Research (NWO) and from the *Centre National d'Etudes Spatiales* (CNES).

References

- Astropy Collaboration, Price-Whelan, A. M., Sipőcz, B. M., et al. 2018, *AJ*, 156, 123
- Astropy Collaboration, Robitaille, T. P., Tollerud, E. J., et al. 2013, *A&A*, 558, A33
- Aumer, M. & Binney, J. J. 2009, *MNRAS*, 397, 1286
- Bailer-Jones, C. A. L., Rybizki, J., Fouesneau, M., Mantelet, G., & Andrae, R. 2018, *AJ*, 156, 58
- Bastian, N. & Lardo, C. 2018, *ARA&A*, 56, 83
- Baumgardt, H. & Makino, J. 2003, *MNRAS*, 340, 227
- Belokurov, V., Evans, N. W., Irwin, M. J., Hewett, P. C., & Wilkinson, M. I. 2006, *ApJ*, 637, L29
- Bergemann, M., Sesar, B., Cohen, J. G., et al. 2018, *Nature*, 555, 334
- Binney, J. 2012, *MNRAS*, 426, 1324
- Bovy, J. 2015, *ApJS*, 216, 29
- Bragaglia, A., Carretta, E., D’Orazi, V., et al. 2017, *A&A*, 607, A44
- Burnett, B. & Binney, J. 2010, *MNRAS*, 407, 339
- Carballo-Bello, J. A., Ramírez Alegría, S., Borissova, J., et al. 2016, *MNRAS*, 462, 501
- Carollo, D., Martell, S. L., Beers, T. C., & Freeman, K. C. 2013, *ApJ*, 769, 87
- Carretta, E., Bragaglia, A., Gratton, R., D’Orazi, V., & Lucatello, S. 2009, *A&A*, 508, 695
- Carretta, E., Bragaglia, A., Gratton, R. G., et al. 2010, *A&A*, 516, A55
- Dallessandro, E., Massari, D., Bellazzini, M., et al. 2014, *ApJ*, 791, L4
- Fernández-Trincado, J. G., Zamora, O., García-Hernández, D. A., et al. 2017, *ApJ*, 846, L2
- Gaia Collaboration, Brown, A. G. A., Vallenari, A., et al. 2018a, *A&A*, 616, A1
- Gaia Collaboration, Helmi, A., van Leeuwen, F., et al. 2018b, *A&A*, 616, A12
- Gómez, F. A., White, S. D. M., Marinacci, F., et al. 2016, *MNRAS*, 456, 2779
- Grillmair, C. J. & Dionatos, O. 2006, *ApJ*, 643, L17
- Harris, W. E. 1996, *AJ*, 112, 1487
- Harris, W. E., Harris, G. L. H., & Alessi, M. 2013, *ApJ*, 772, 82
- Helmi, A. & White, S. D. M. 1999, *MNRAS*, 307, 495
- Ibata, R., Malhan, K., & Martin, N. 2019, arXiv e-prints
- Ibata, R. A., Malhan, K., Martin, N. F., & Starkenburg, E. 2018, *ApJ*, 865, 85
- Kirby, E. N., Simon, J. D., & Cohen, J. G. 2015, *ApJ*, 810, 56
- Kruijssen, J. M. D. 2015, *MNRAS*, 454, 1658
- Laporte, C. F. P., Johnston, K. V., Gómez, F. A., Garavito-Camargo, N., & Besla, G. 2018, *MNRAS*, 481, 286
- Lindgren, L., Hernández, J., Bombrun, A., et al. 2018, *A&A*, 616, A2
- Lucatello, S., Tsangarides, S., Beers, T. C., et al. 2005, *ApJ*, 625, 825
- Martell, S. L. & Grebel, E. K. 2010, *A&A*, 519, A14
- Martell, S. L., Smolinski, J. P., Beers, T. C., & Grebel, E. K. 2011, *A&A*, 534, A136
- McMillan, P. J. 2017, *MNRAS*, 465, 76
- Milone, A. P., Piotto, G., Renzini, A., et al. 2017, *MNRAS*, 464, 3636
- Odenkirchen, M., Grebel, E. K., Dehnen, W., et al. 2003, *AJ*, 126, 2385
- Pietrinferni, A., Cassisi, S., Salaris, M., & Castelli, F. 2006, *ApJ*, 642, 797
- Piffl, T., Binney, J., McMillan, P. J., et al. 2014, *MNRAS*, 445, 3133
- Posti, L. & Helmi, A. 2019, *A&A*, 621, A56
- Renzini, A., D’Antona, F., Cassisi, S., et al. 2015, *MNRAS*, 454, 4197
- Rockosi, C. M., Odenkirchen, M., Grebel, E. K., et al. 2002, *AJ*, 124, 349
- Schiavon, R. P., Zamora, O., Carrera, R., et al. 2017, *MNRAS*, 465, 501
- Schönrich, R., Binney, J., & Dehnen, W. 2010, *MNRAS*, 403, 1829
- Shipp, N., Drlica-Wagner, A., Balbinot, E., et al. 2018, *ApJ*, 862, 114
- Simpson, J. D., De Silva, G., Martell, S. L., Navin, C. A., & Zucker, D. B. 2017, *MNRAS*, 472, 2856
- Starkenburg, E., Shetrone, M. D., McConnachie, A. W., & Venn, K. A. 2014, *MNRAS*, 441, 1217
- Tang, B., Liu, C., Fernández-Trincado, J. G., et al. 2019, *ApJ*, 871, 58
- Vasiliev, E. 2019a, *MNRAS*, 482, 1525
- Vasiliev, E. 2019b, *MNRAS*, 484, 2832
- Watkins, L. L., van der Marel, R. P., Sohn, S. T., & Evans, N. W. 2018, arXiv e-prints
- Yanny, B., Rockosi, C., Newberg, H. J., et al. 2009, *AJ*, 137, 4377

Appendix A: Candidate star-cluster associations

Table A.1: Possible star-cluster associations based on the orbital actions and metallicity. The columns list the star and cluster IDs, the degree of confidence for the orbital association rejection, and the absolute difference in metallicity. Entries in bold are the associations that can be excluded at less than 68% confidence level.

Star ID	Cluster	Confidence level	$ \Delta[Fe/H] $
J115957.53+044724.6	NGC1261	85.3%	0.095
J115957.53+044724.6	NGC1851	83.8%	0.185
J115957.53+044724.6	NGC6229	94.1%	0.066
J115957.53+044724.6	NGC6864	94.9%	0.075
J115957.53+044724.6	NGC6981	92.3%	0.116
J224241.48+131459.2	NGC362	88.9%	0.130
J224241.48+131459.2	NGC1261	47.8%	0.100
J224241.48+131459.2	NGC1851	75.6%	0.010
J224241.48+131459.2	NGC5904	88.5%	0.160
J224241.48+131459.2	NGC6864	24.9%	0.120
J160327.56+173348.5	NGC288	67.9%	0.182
J160327.56+173348.5	NGC6723	94.9%	0.038
J083423.50+124324.4	NGC1851	77.7%	0.186
J083423.50+124324.4	NGC2808	89.9%	0.186
J115826.53+043047.8	NGC1904	85.8%	0.092
J115826.53+043047.8	NGC4147	90.1%	0.108
J115826.53+043047.8	NGC5286	93.9%	0.028
J115826.53+043047.8	ESO280-6	88.8%	0.098
J115826.53+043047.8	NGC6584	91.3%	0.172
J115826.53+043047.8	NGC6981	80.8%	0.192
J115826.53+043047.8	NGC7089	77.8%	0.012
J115826.53+043047.8	NGC7492	94.0%	0.018
J162242.14+315035.7	NGC6205	80.5%	0.026
J085455.54+372927.9	NGC1261	90.3%	0.191
J085455.54+372927.9	NGC1851	83.1%	0.101
J085455.54+372927.9	NGC2808	86.4%	0.101
J161013.43+052403.6	NGC6723	93.2%	0.100
J102826.25+175448.9	NGC362	25.4%	0.122
J161943.91+163110.9	NGC288	94.9%	0.190
J161943.91+163110.9	NGC6284	77.7%	0.199
J105019.09+005105.6	NGC5904	90.6%	0.079
J152635.55+510607.6	NGC288	74.0%	0.156
J085342.07+364723.9	NGC362	55.8%	0.051
J085342.07+364723.9	NGC1261	91.2%	0.021
J085342.07+364723.9	NGC1851	93.2%	0.069
J085342.07+364723.9	NGC2808	62.4%	0.069
J085342.07+364723.9	NGC5904	91.8%	0.081
J085342.07+364723.9	NGC6121	90.8%	0.069
J085342.07+364723.9	NGC6284	90.4%	0.061
J085342.07+364723.9	NGC6864	60.0%	0.041
J014924.75+150045.4	NGC288	94.4%	0.110
J014924.75+150045.4	NGC362	80.4%	0.123
J014924.75+150045.4	NGC5946	93.8%	0.140
J014924.75+150045.4	NGC6205	84.1%	0.150
J014924.75+150045.4	NGC6284	82.8%	0.120
J014924.75+150045.4	NGC6544	83.3%	0.040
J014924.75+150045.4	NGC6681	86.6%	0.190
J160709.22+044712.6	NGC6681	94.0%	0.017
J173052.92+333303.1	NGC6205	65.0%	0.006
J172931.11+264940.2	Pal15	92.4%	0.068
J234549.70+005055.9	NGC2298	44.9%	0.155
J234549.70+005055.9	NGC5286	72.0%	0.106
J234549.70+005055.9	NGC5634	92.2%	0.125
J234549.70+005055.9	IC4499	75.0%	0.186
J234549.70+005055.9	IC1257	62.8%	0.136
J234549.70+005055.9	ESO280-06	92.3%	0.036
J234549.70+005055.9	NGC6779	71.9%	0.195
J234549.70+005055.9	NGC7089	69.5%	0.146
J234549.70+005055.9	NGC7492	85.4%	0.116
J125224.31+193358.3	NGC2298	93.6%	0.100
J125224.31+193358.3	NGC4147	72.7%	0.080
J125224.31+193358.3	NGC7492	88.4%	0.170
J131447.33+010356.4	NGC5897	54.9%	0.097

Appendix B: Orbits of the CN-strong stars

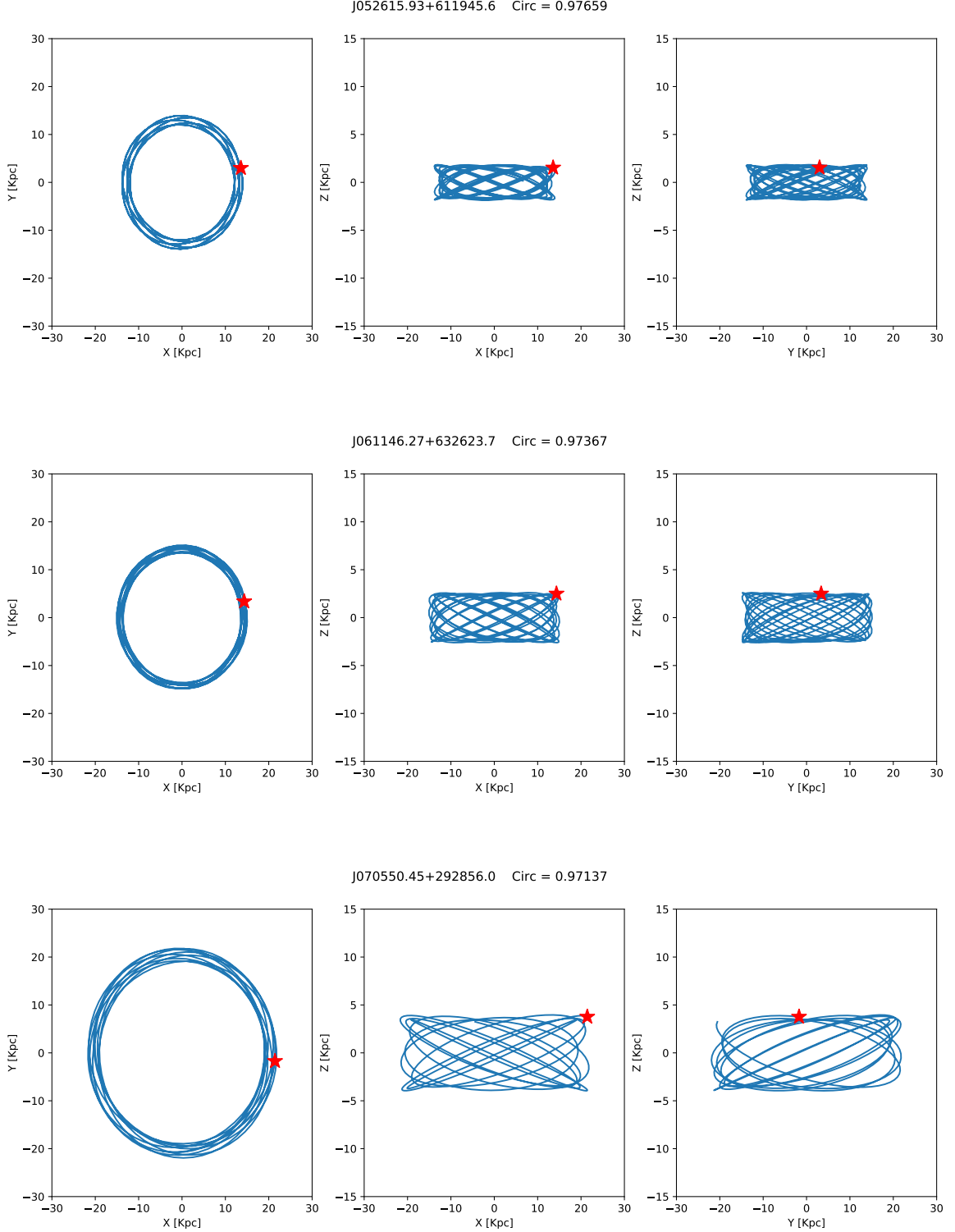


Fig. B.1: Projection, in the three galactocentric cartesian planes of the reconstructed orbit for the CN-strong stars used in this study, ordered by decreasing absolute value of circularity. The red star indicates the current position of the star in the Galaxy. The star ID and the circularity are given above each set of panels.

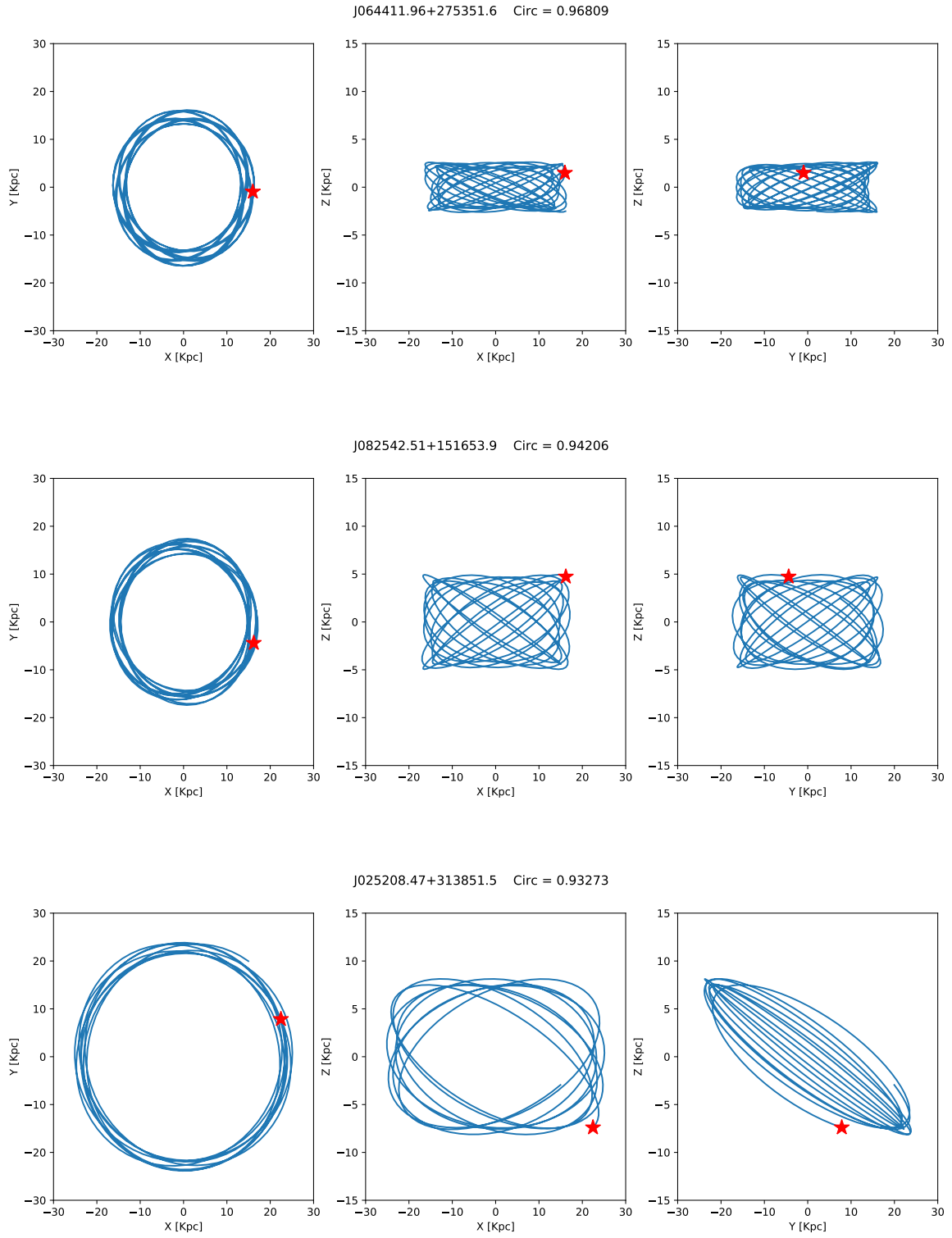


Fig. B.1: Continued.

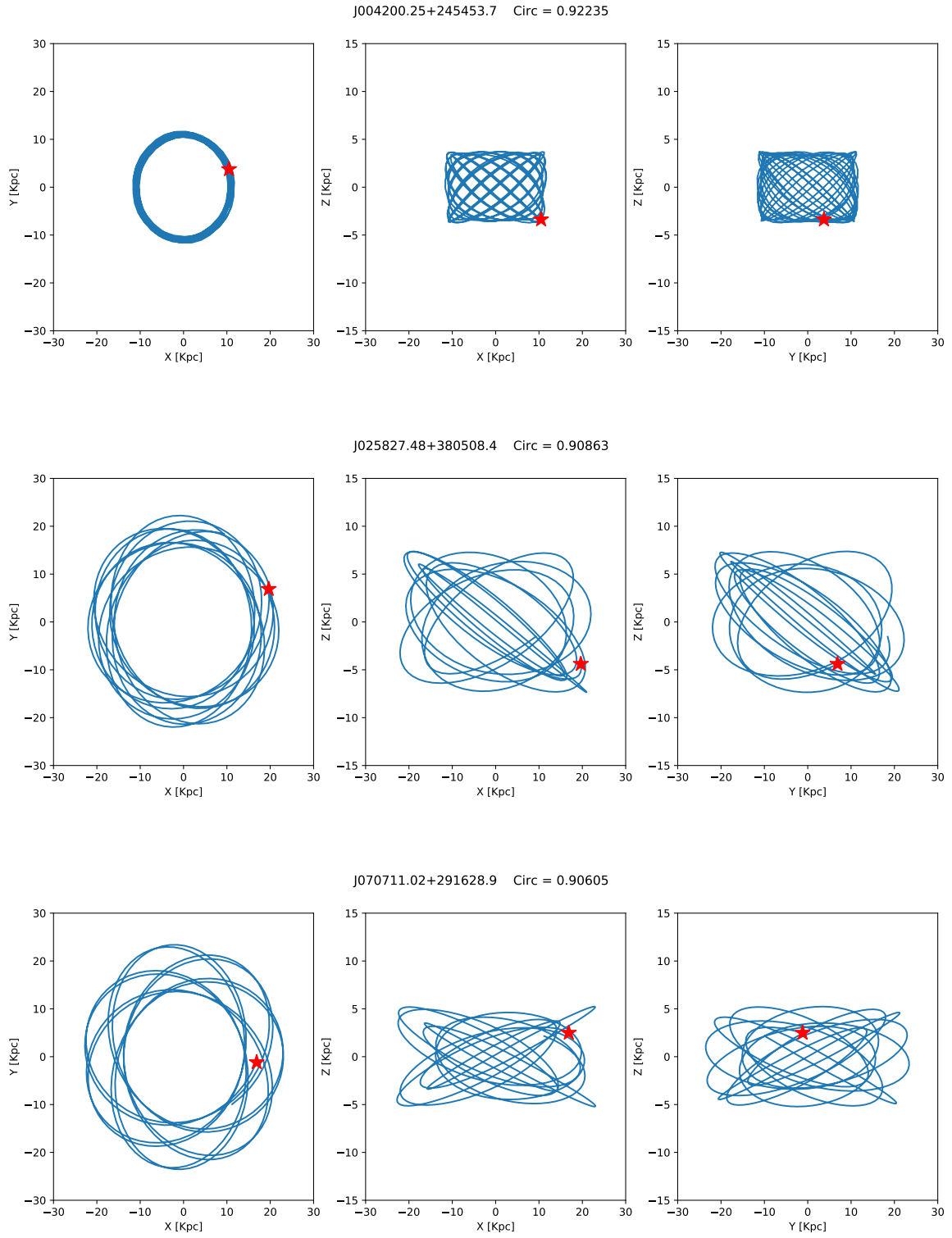


Fig. B.1: Continued.

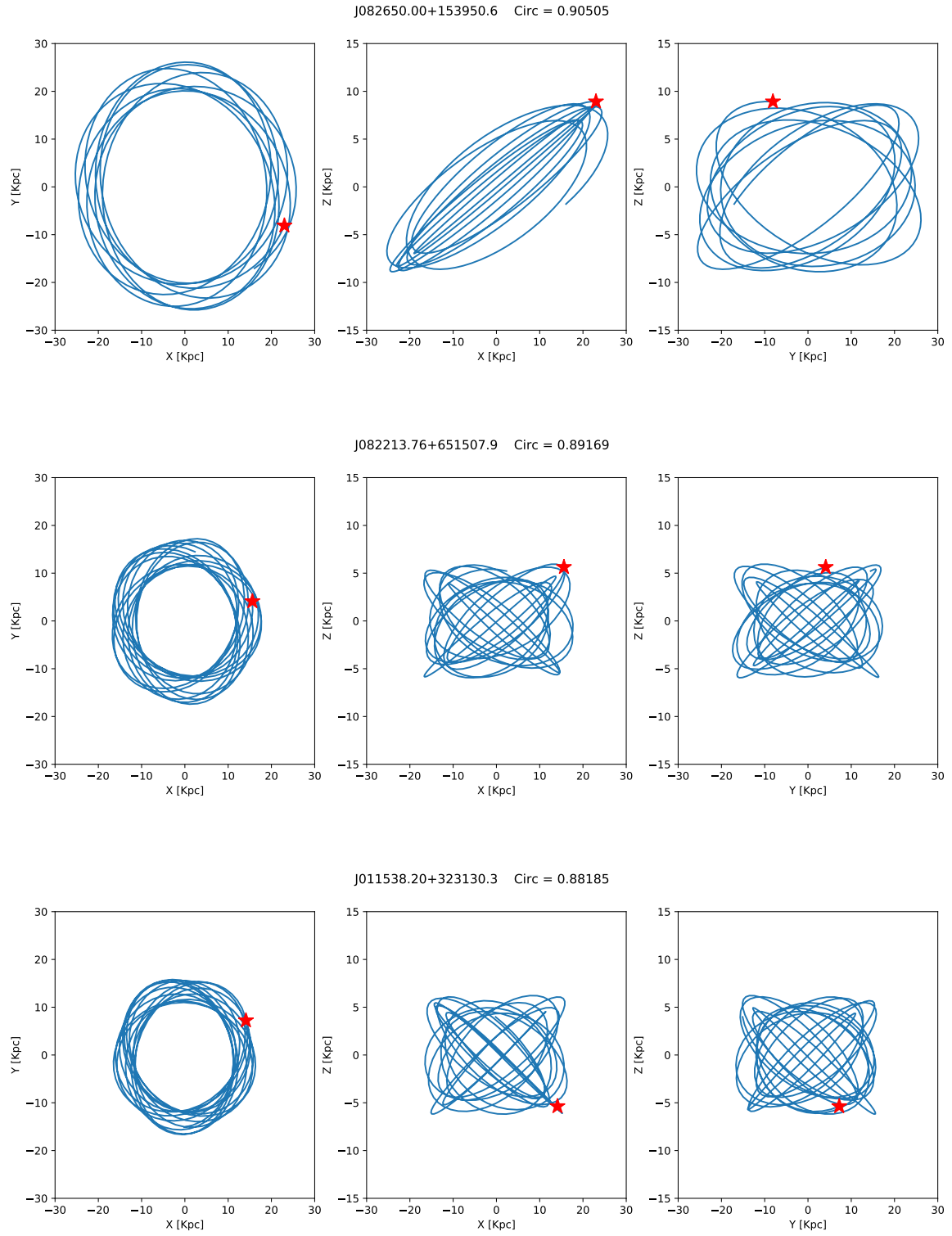


Fig. B.1: Continued.

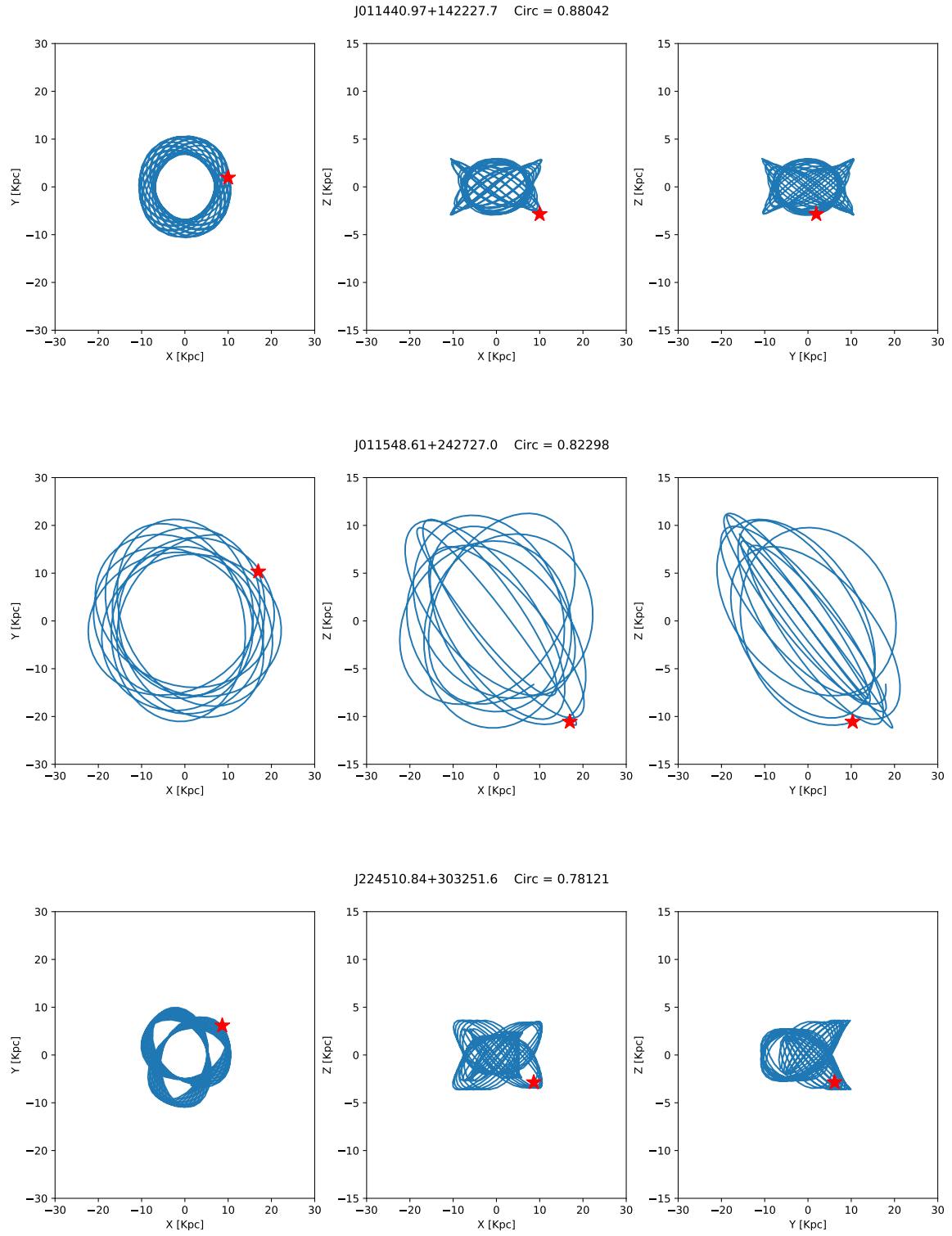


Fig. B.1: Continued.

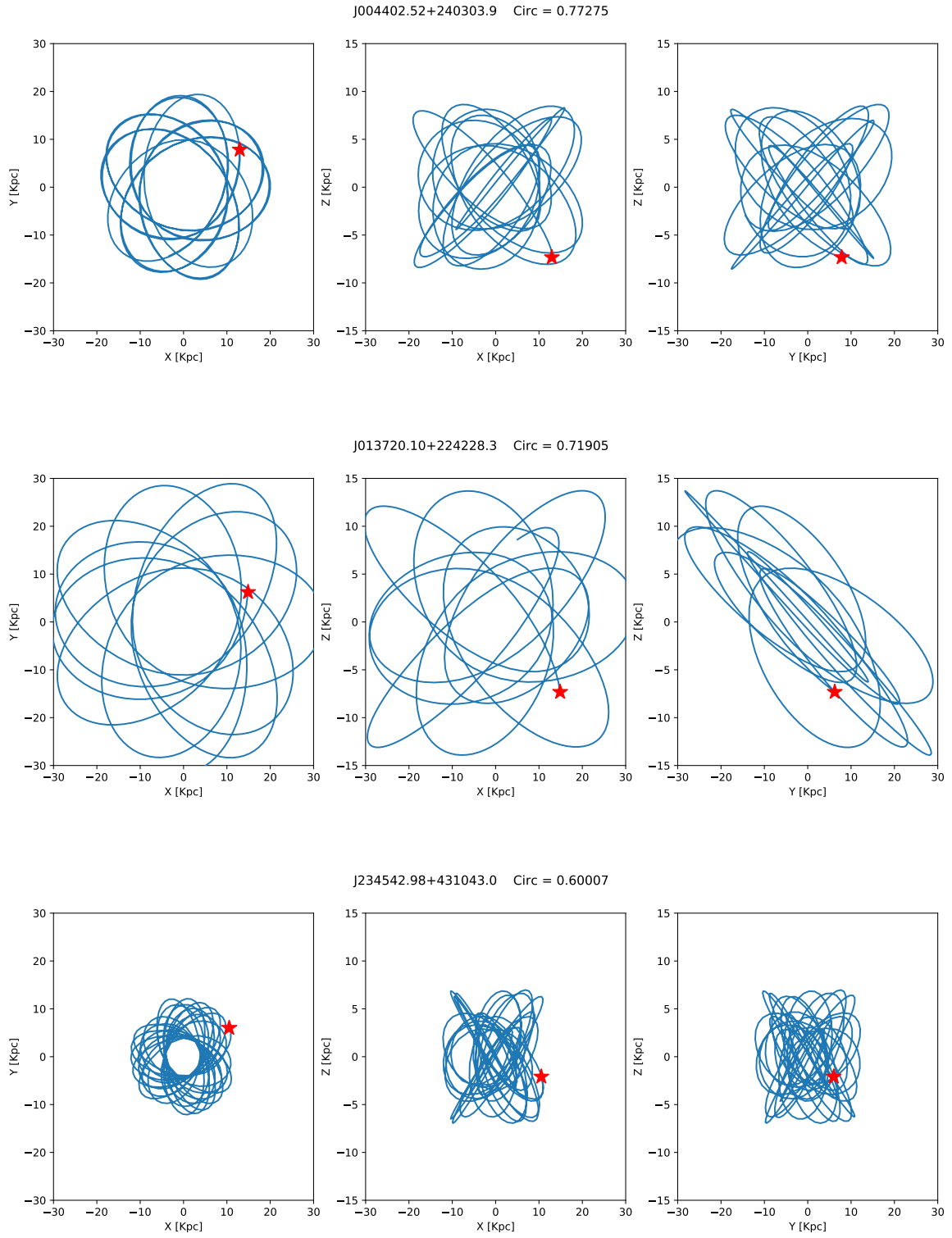


Fig. B.1: Continued.

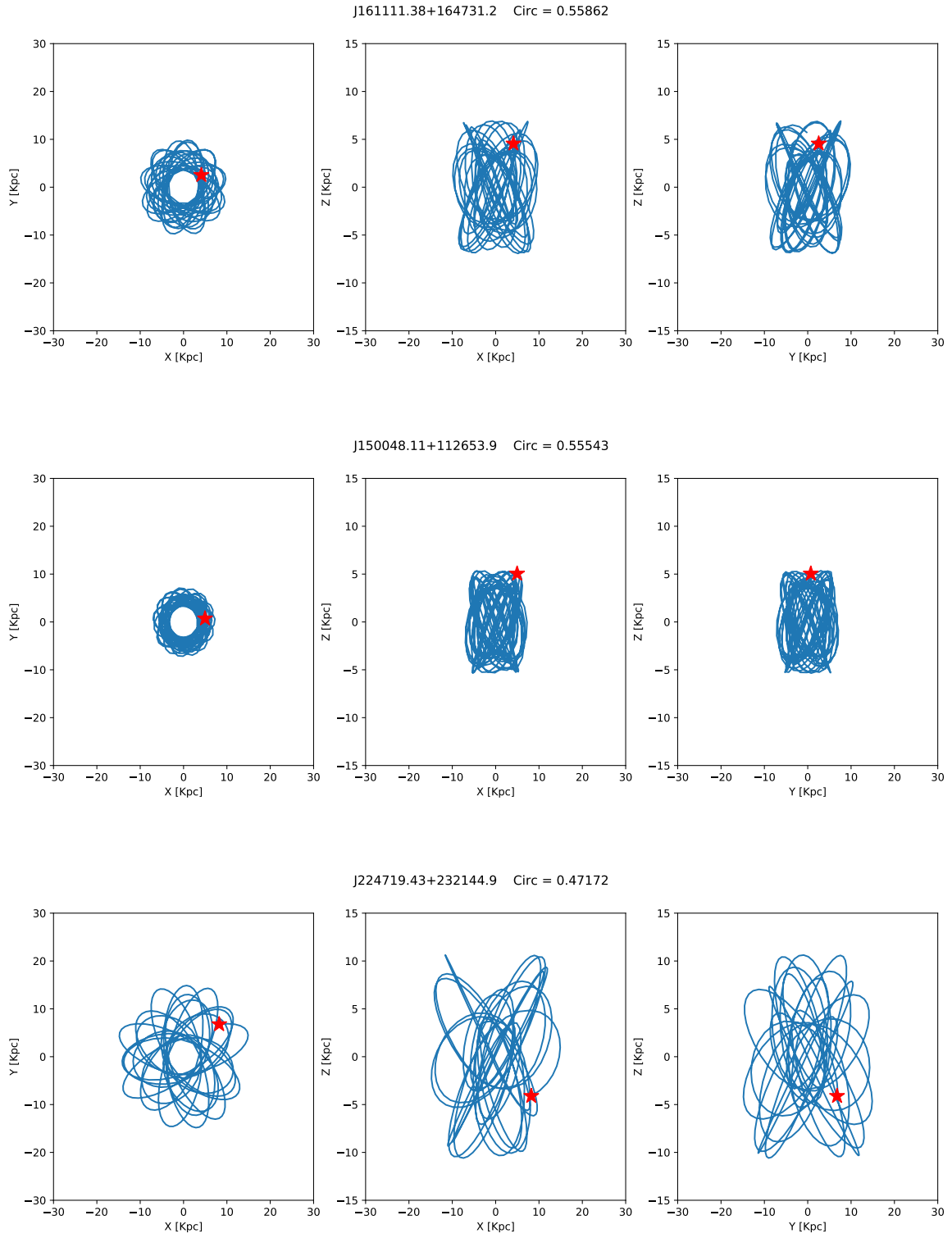


Fig. B.1: Continued.

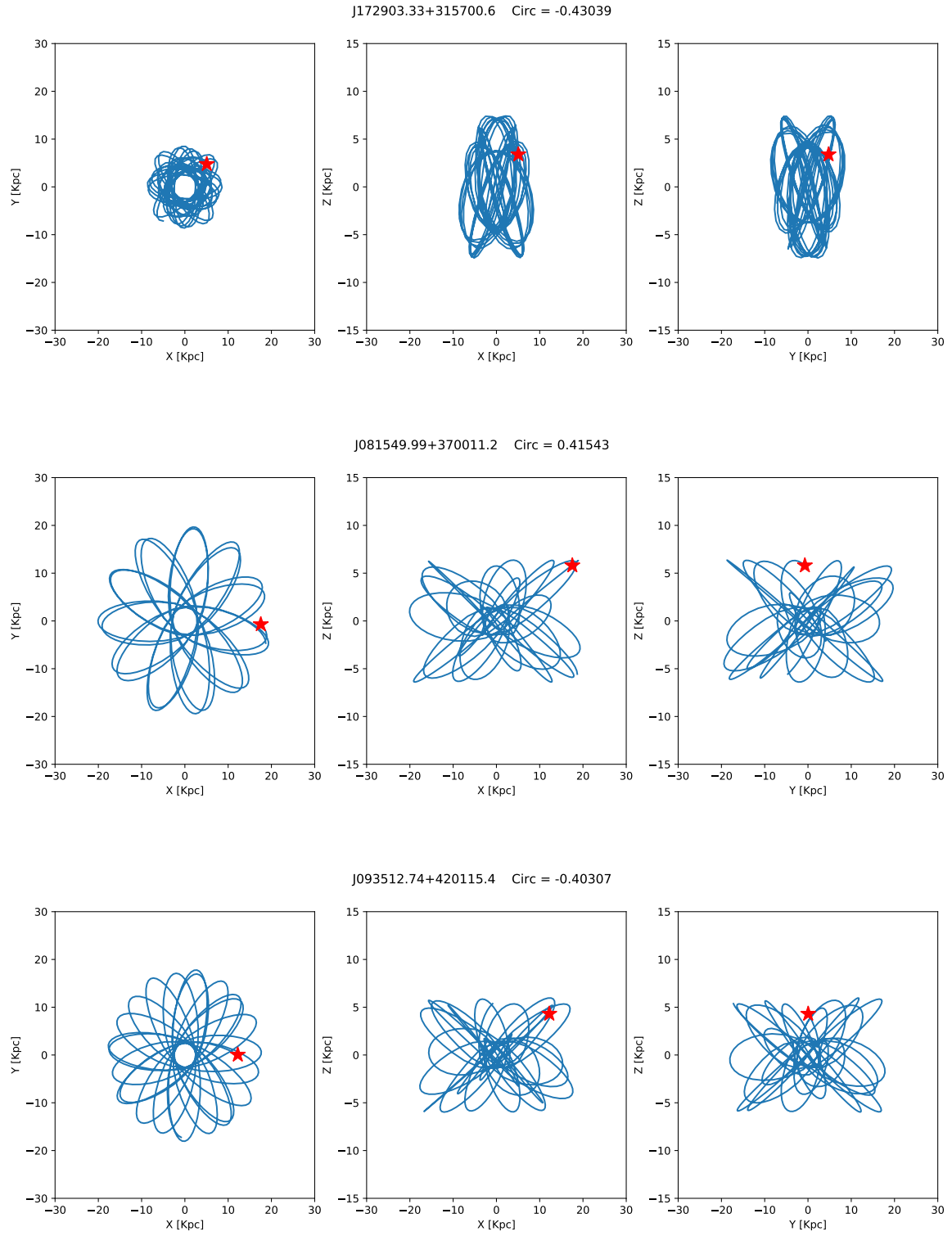


Fig. B.1: Continued.

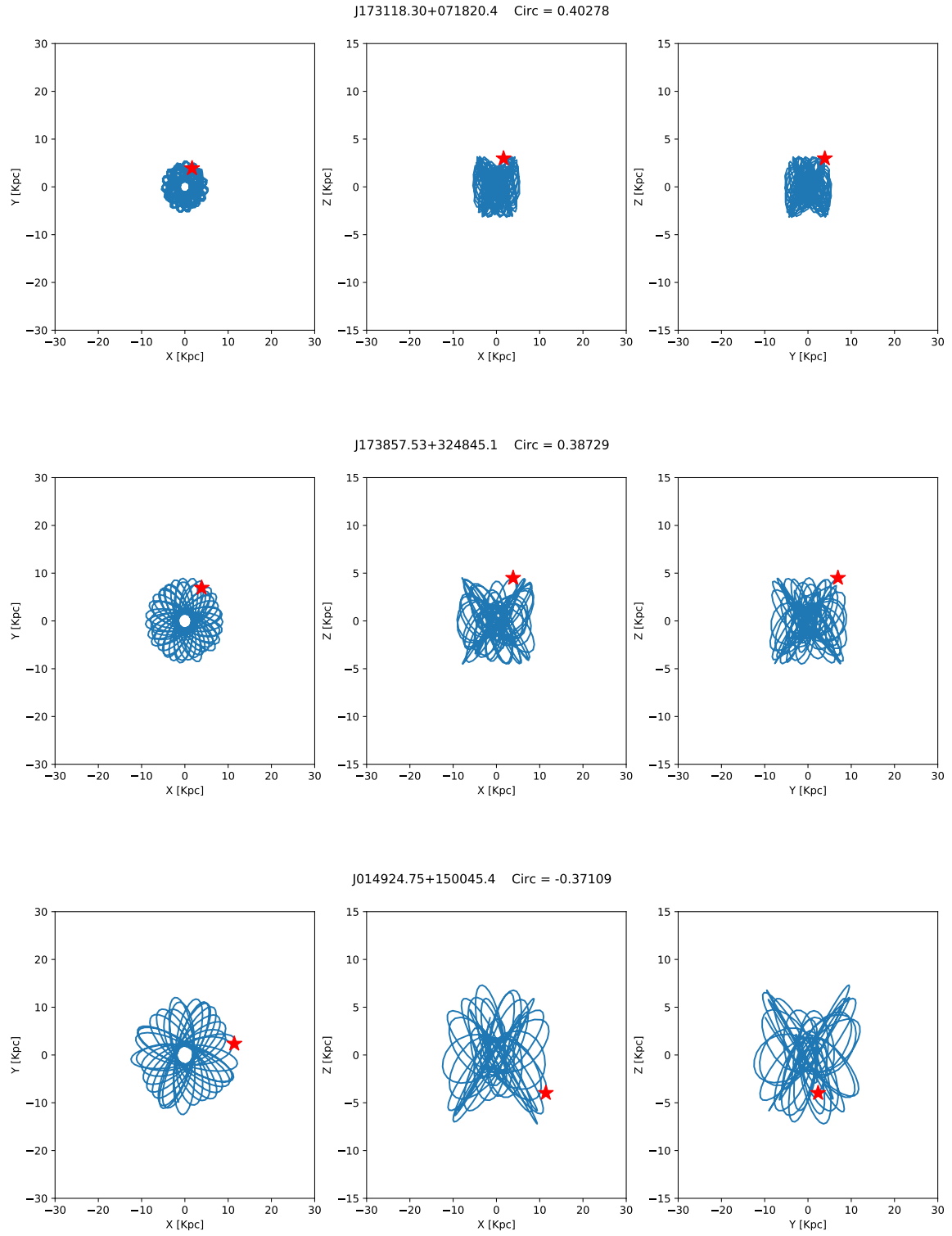


Fig. B.1: Continued.

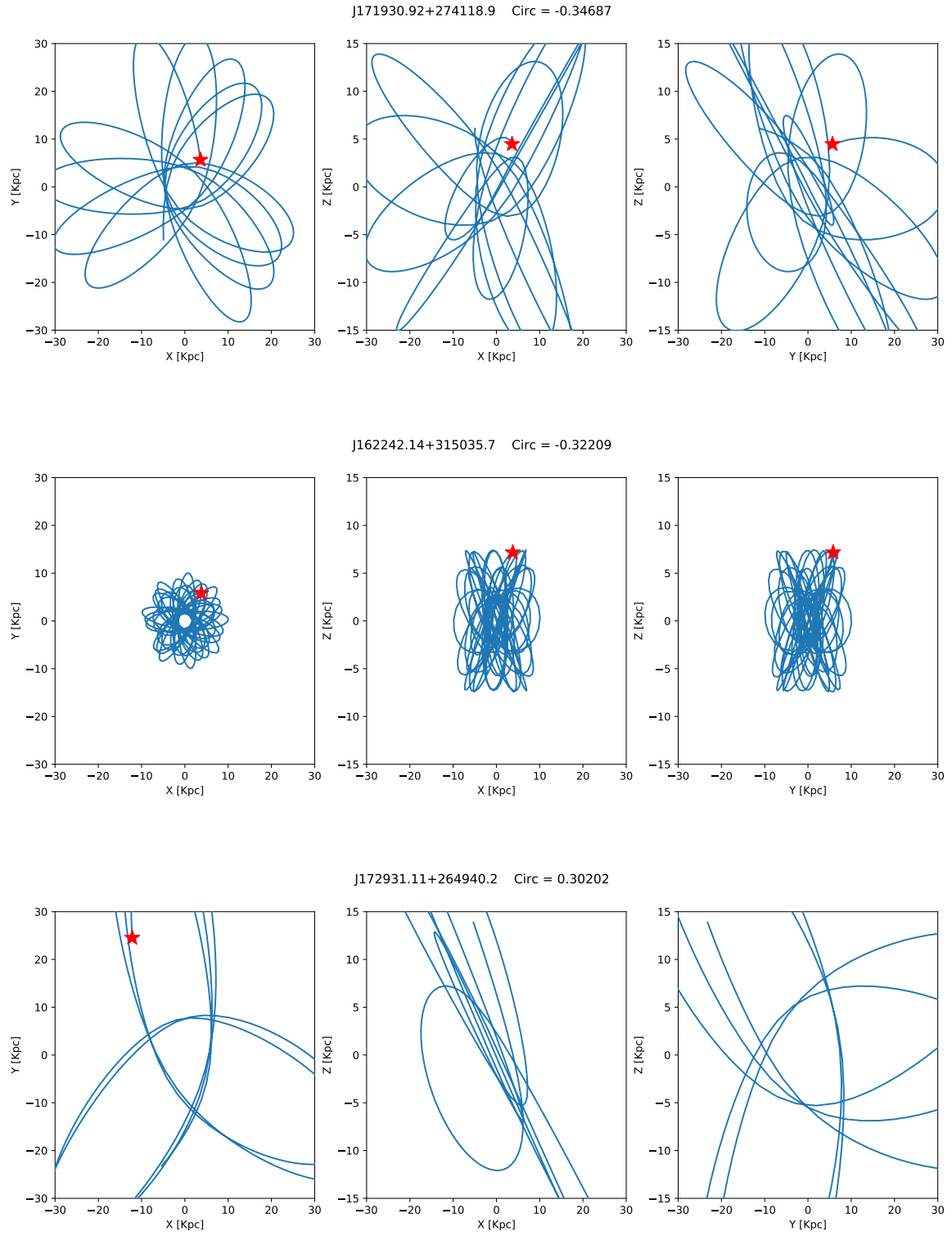


Fig. B.1: Continued.

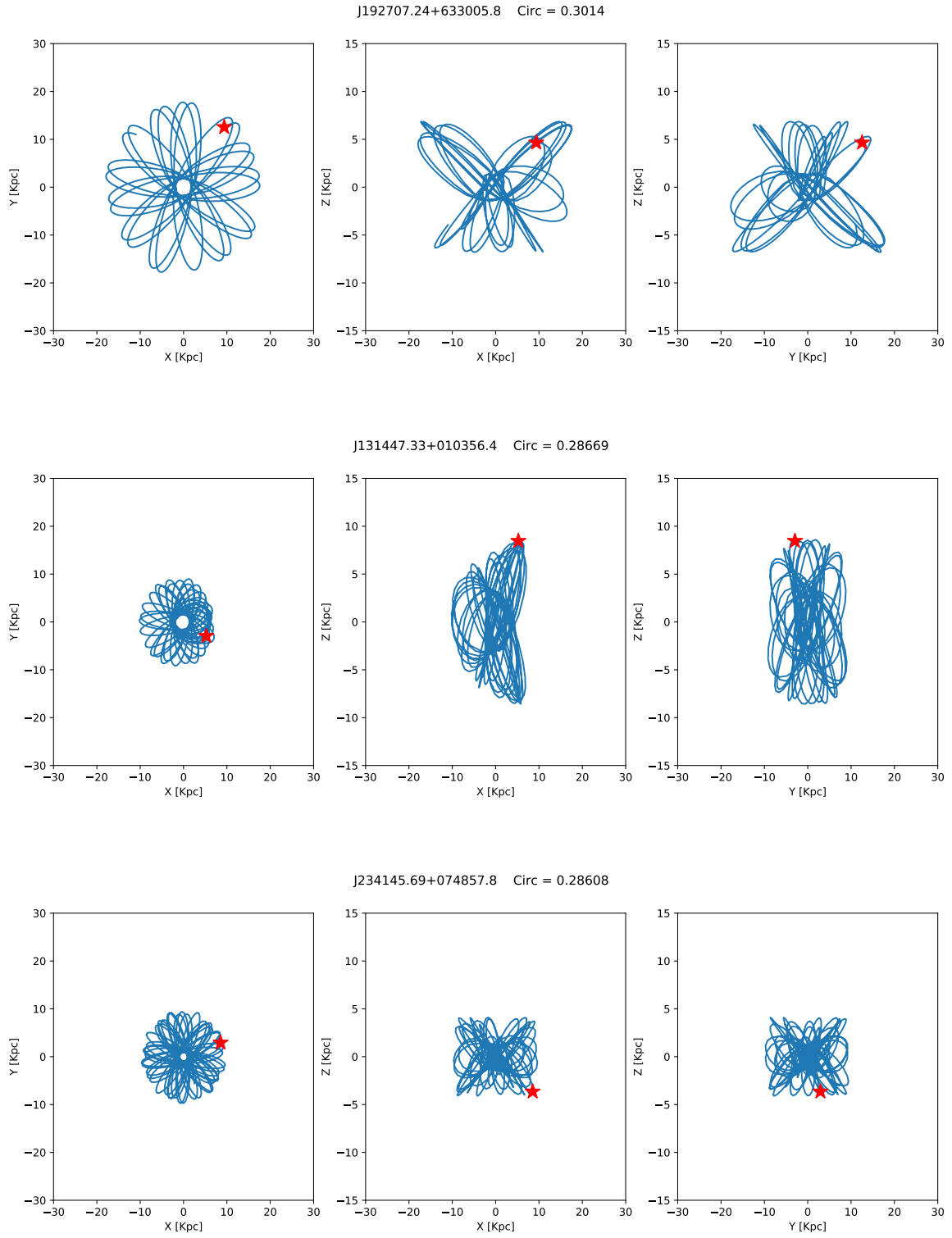


Fig. B.1: Continued.

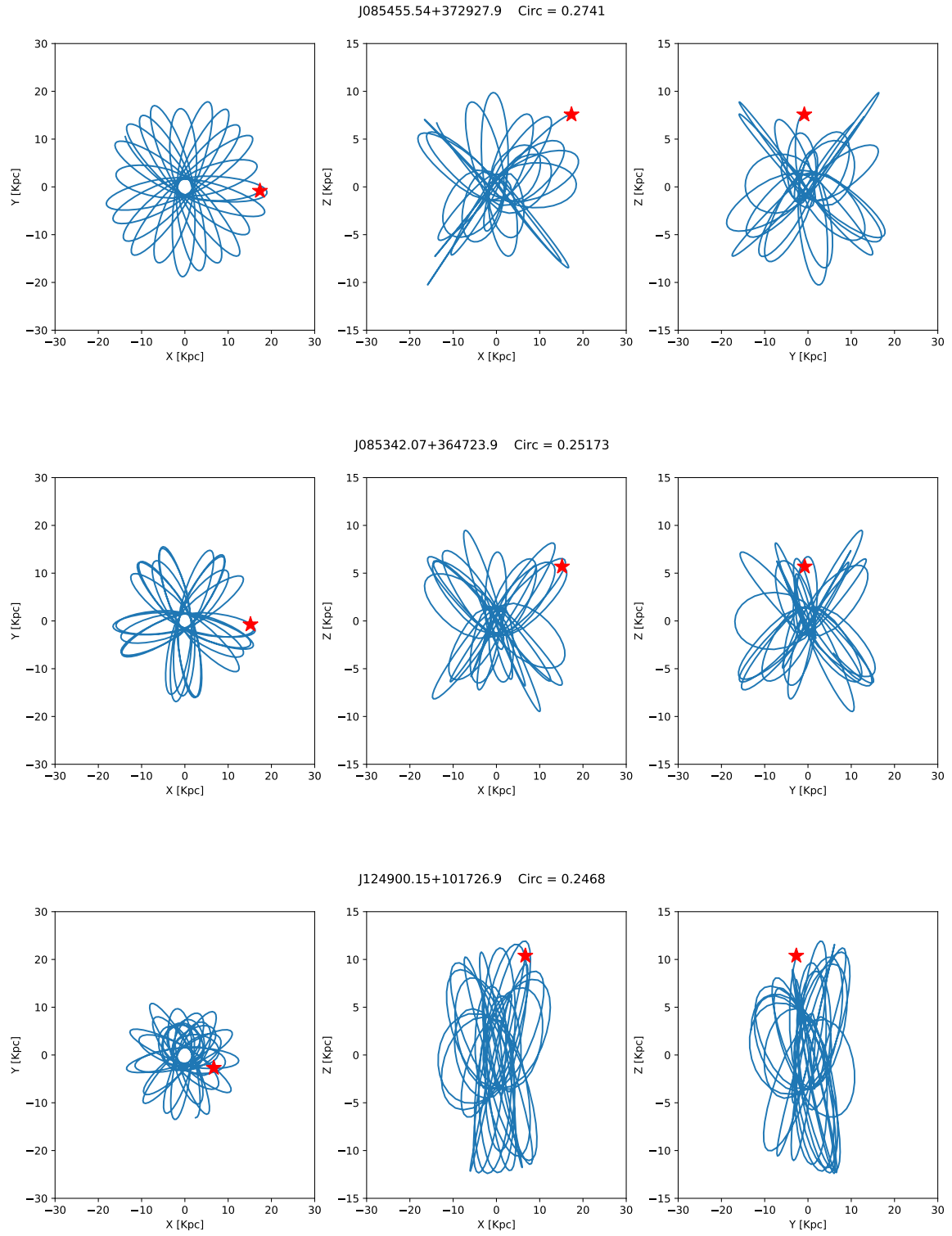


Fig. B.1: Continued.

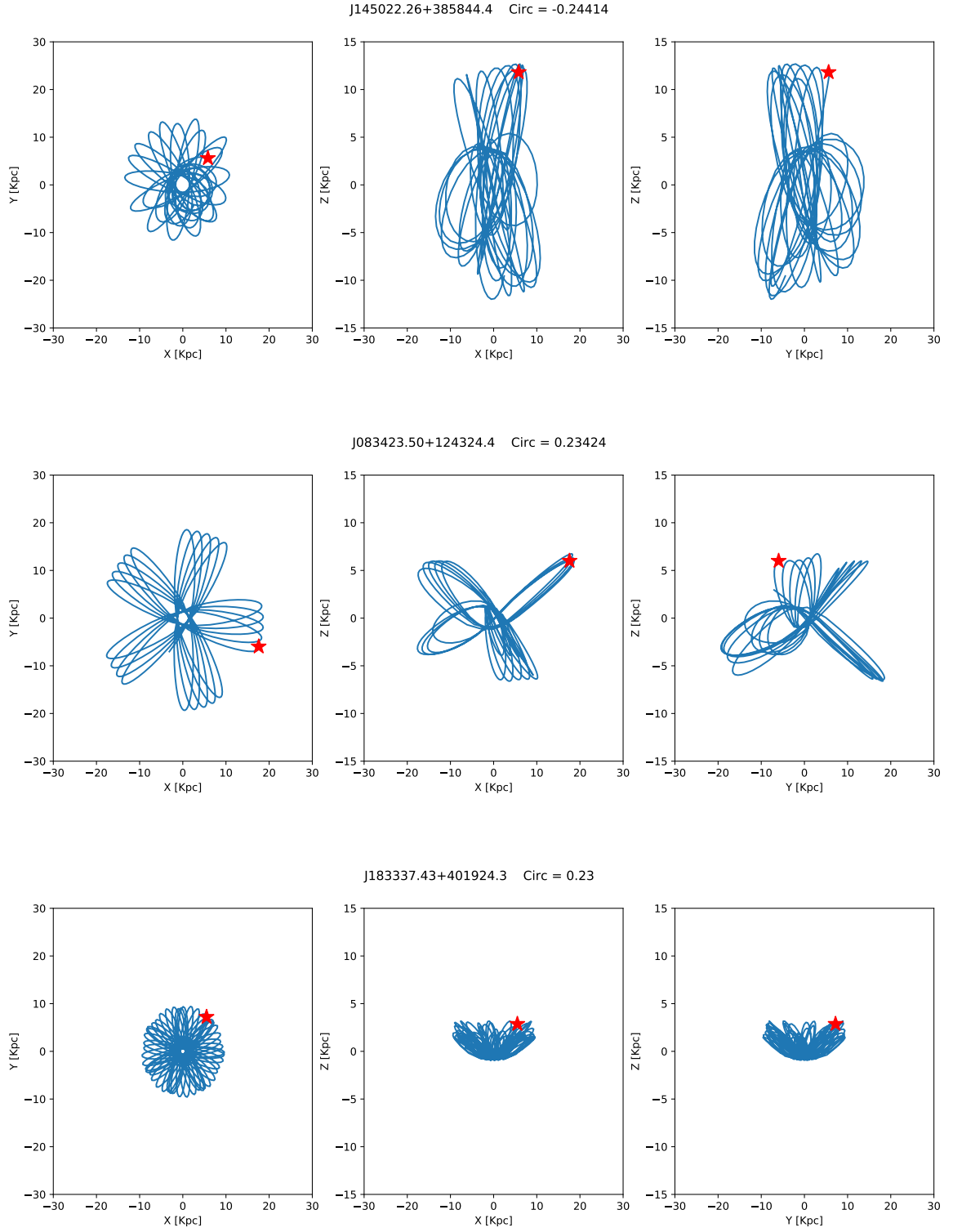


Fig. B.1: Continued.

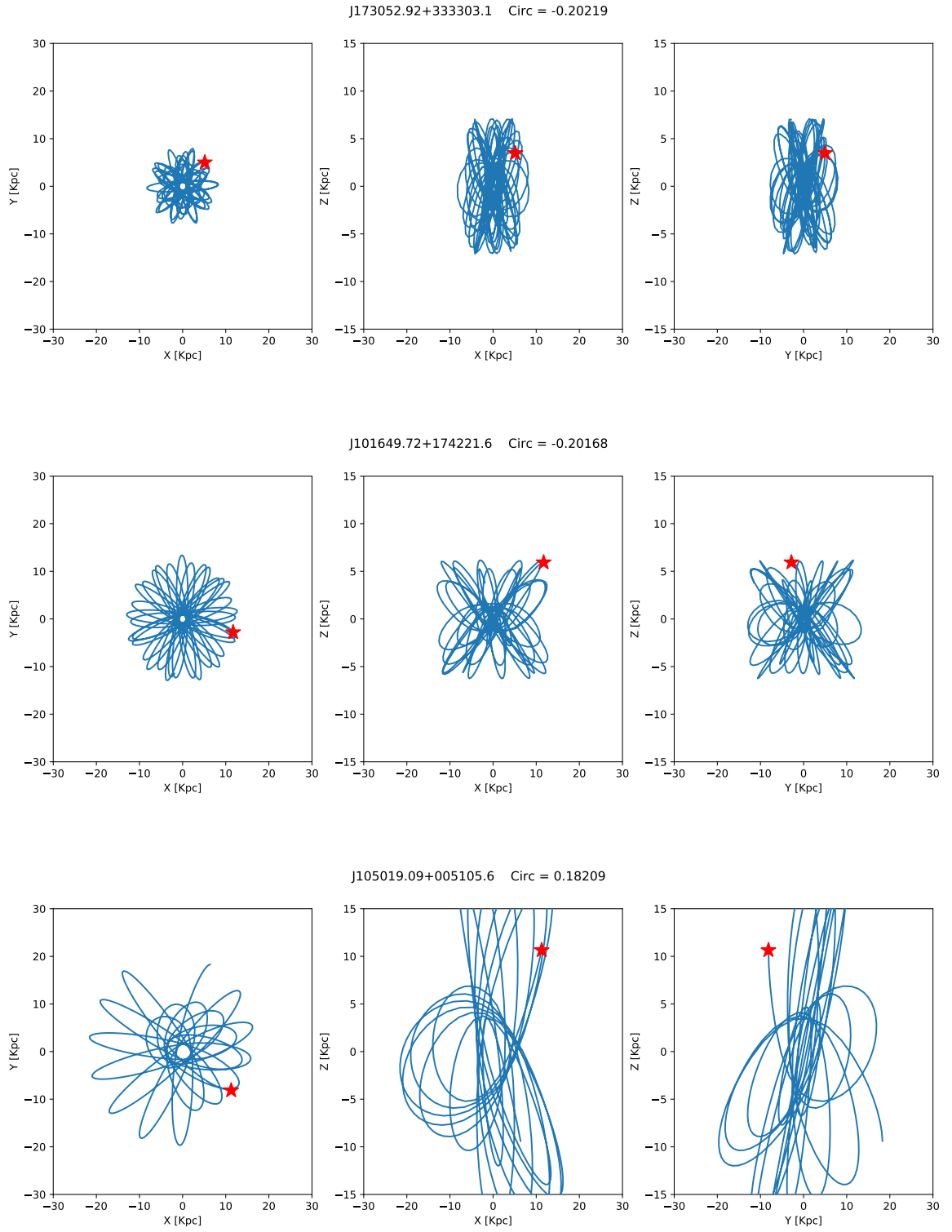


Fig. B.1: Continued.

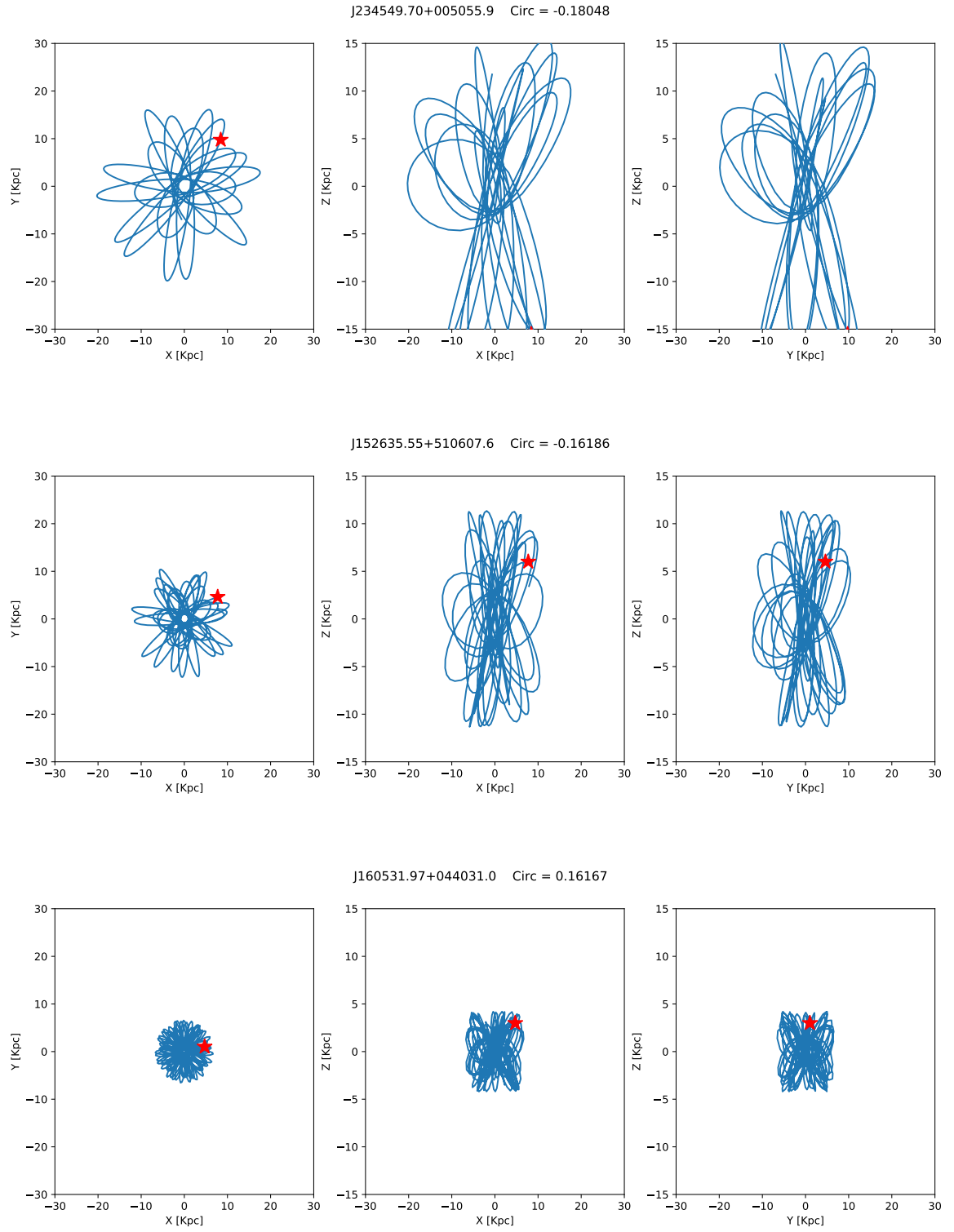


Fig. B.1: Continued.

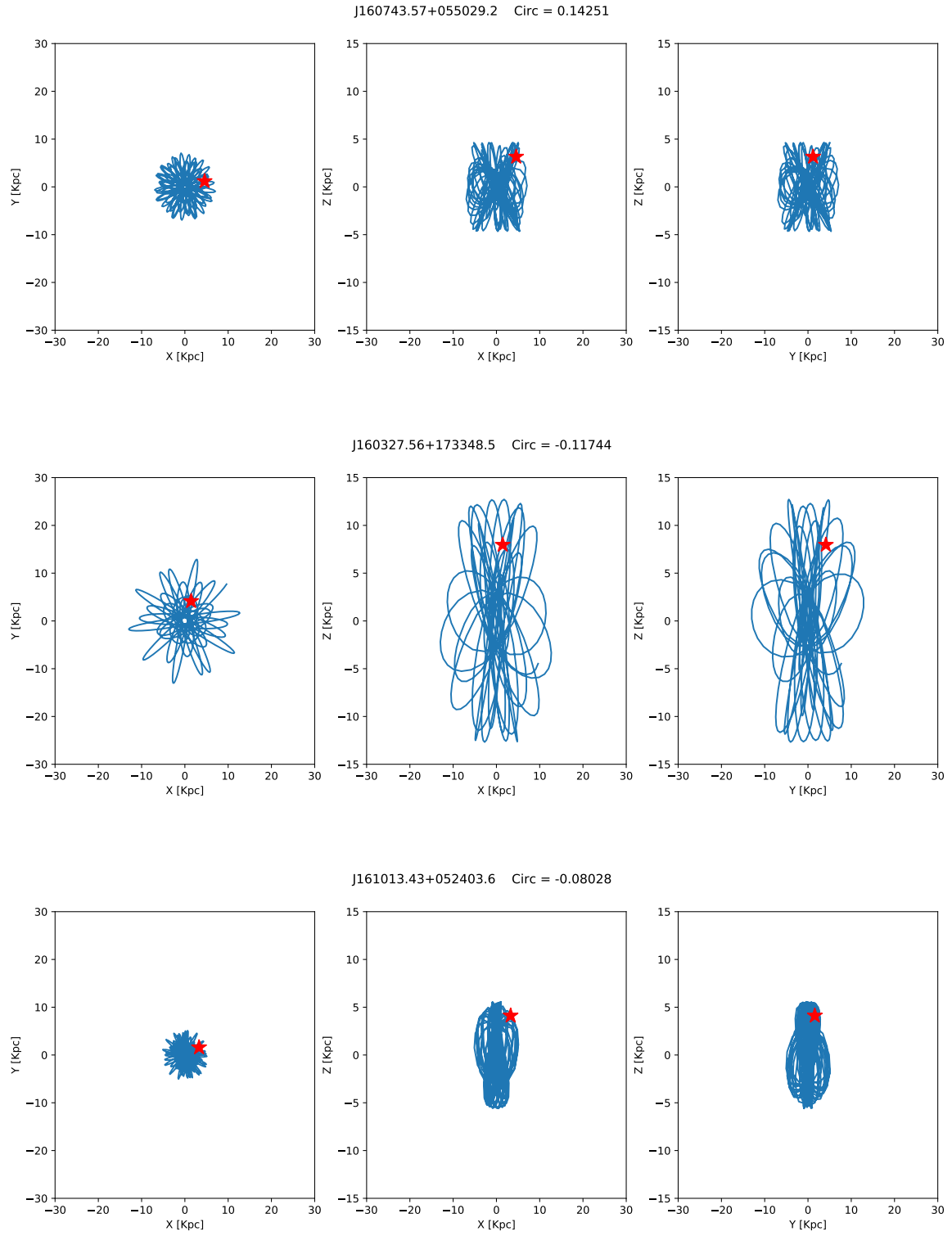


Fig. B.1: Continued.

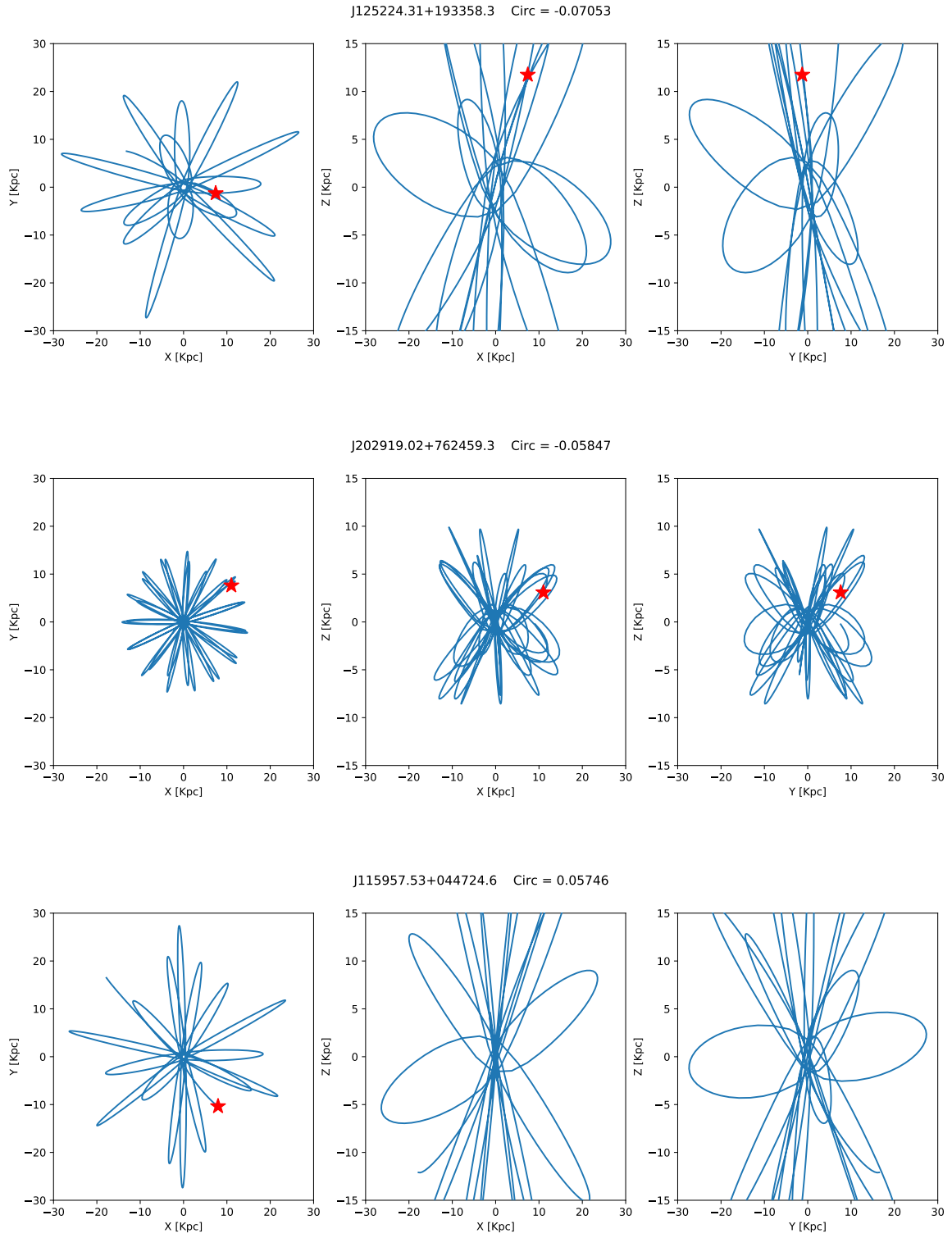


Fig. B.1: Continued.

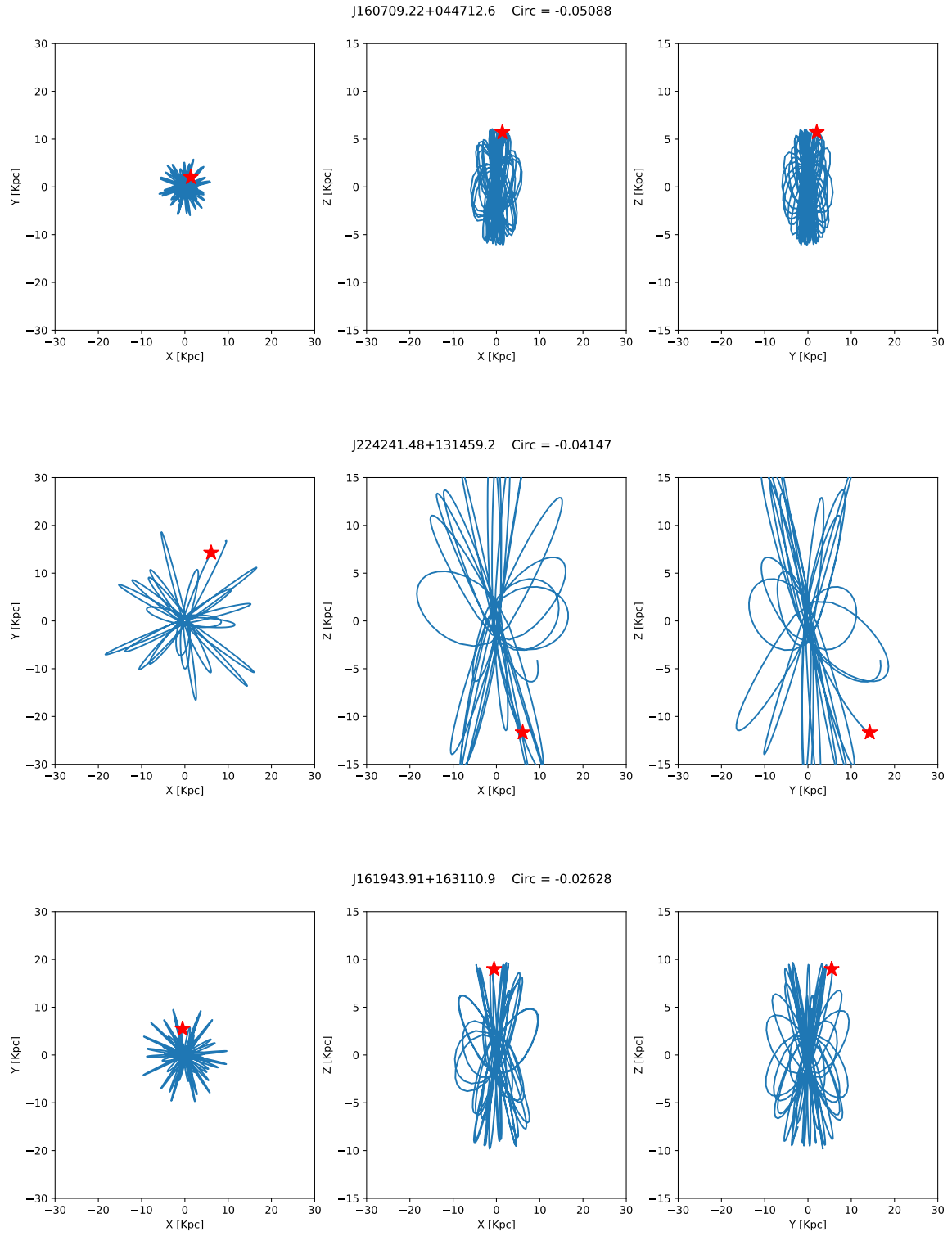


Fig. B.1: Continued.